ELSEVIER

Contents lists available at ScienceDirect

Flow Measurement and Instrumentation

journal homepage: www.elsevier.com/locate/flowmeasinst





Measuring the viscoelastic behavior of dilute polymer solutions using high-speed statistical particle microrheology

Zijie Qu^{a,*}, Xiongfeng Yi^b, Kenneth S. Breuer^c

- a UM-SJTU Joint Institute, Shanghai Jiao Tong University, Shanghai, 200240, China
- ^b Brown University, School of Engineering, 4726 Calhoun Road, Houston TX 77204, USA
- ^c Brown University, School of Engineering, 184 Hope St, Providence, RI 02912, USA

ARTICLE INFO

Keywords: Viscoelasticity Microrheology Statistical particle tracking velocimetry

ABSTRACT

The viscoelastic behavior of polymer solutions is commonly measured using oscillating shear rheometry, however, the accuracy of such methods is limited by the oscillating frequency of the equipment and since the relaxation time of the dilute polymer solutions is short, this requires measurement at very high frequencies. Microrheology has been proposed to overcome this technical challenge. Yet the equipment for resolving the statistics of particle displacements in microrheology is expensive. In this work, we measured the viscoelastic behavior of Methocel solutions at various concentrations using a conventional epi-fluorescence microscope coupled to a high-speed intensified camera. Statistical Particle Tracking is used in analyzing the mean-squared displacement of the dispersive particles. Relaxation times ranging from 0.76 - 9.00 ms and viscoelastic moduli, G' between 11.34 and 3.39 are reported for Methocel solutions of concentrations between 0.063 - 0.5%.

1. Introduction

The rheology of complex fluids has been studied extensively through the last few decades [1-3]. It is highly relevant to not only industrial applications, such as paints [4], plastics [5] and printing inks [6], but also to many research areas especially biological applications and processing [7,8]. The rheological properties, especially the viscoelasticity of complex fluids, give important details on micro-structural features and dynamics of the system [9]. In general, the relaxation time of the system varies and spans a large range of time scales depending on the viscoelastic modulus (G' and G'') [10,11]. For dilute polymer solutions with a small molecule size, the relaxation time is usually short. Measurements with high frequency are thus indispensable to resolve their rheological behavior [12,13].

The viscoelastic behavior of such solutions can be measured using an oscillating shear rheometer [14,15], which requires a precise and sensitive measurement of the torque of the shear plate at a high frequency, and is difficult to achieve using a conventional rheometer [15]. In contrast, microrheology measures the rheological properties using the motion of particles or colloidal probes that are suspended in the fluid. Such an approach dates back decades [16]. One pivotal moment in the history of microrheology measurement technique and theory occurred in 1995 when Mason and Weitz [17,18] showed that the linear viscoelastic properties of the fluid could be measured by tracking the thermal fluctuations of well-defined particles. Using the

generalized Stokes–Einstein relation, the linear viscoelastic property is quantified by the mean-squared displacement (MSD) of the particles. Over many years, several measurement techniques have been proposed to determine the MSD of particle dispersion including the light-scattering technique [12], laser microscopy technique [19], etc. In addition, video-based particle-tracking microscopy [20] has also been applied in microrheology experiments and has grown rapidly in recent years as imaging technology has improved.

In most particle-tracking microscopy based microrheology measurements, the MSD is processed by measuring the displacement of particle at different times. This is achieved by comparing the location of particles in the video at various frames using image post processing. Hence, it is expected that the accuracy of such measurement decreases at high frame rate. Camera noise, especially generated from CMOS cameras, including general Gaussian noise [21], photon shot noise [22] and signal read noise becomes more severe as the image acquisition frequency increases. An image intensifier is capable of detecting and amplifying low-light-level images to overcome the limited exposure at high frame rate for fluorescent systems [23]. But the intensifier introduces additional noise to the resultant images. All these noisy signals may lead to a false measurements of particle displacements during image post-processing. In addition to optical noise, the overlapping of particles due to high dispersion can also bring difficulties in displacement detection [24].

E-mail address: zijie.qu@sjtu.edu.cn (Z. Qu).

^{*} Corresponding author.

Another drawback of traditional particle displacement detection is that it requires a precise particle-to-particle matching between frames. The most widely used algorithm for particle matching is nearest-neighbor matching [25], which however does not guarantee a correct match and becomes less accurate with all the false signals introduced at high frame rates. Even in dilute particle suspensions, it is possible that multiple particles cluster locally and the nearest-neighbor algorithm will not lead to a one-to-one matching. Particles may also disperse out of focus or outside the observation window such that a particle pair does not exist. For images taken at high frequency, some background noise can be detected as "particles" and these random appearances break the one-to-one matching required for the nearest neighbor algorithm.

To address these issues when measuring the MSD at high frequency, Statistical Particle Tracking Velocimetry (SPTV) technique [24] can be applied to the image post-processing. With a similar approach, SPTV requires all particles in each frame to be detected using intensity threshold [26] or diffraction ring [27]. Instead of finding a precise one-to-one particle matching, SPTV purposely utilizes a large interrogation window to include multiple tracer particles (including noise "particles") and measures the displacement distribution. Drop-in and drop-out particles, due to dispersion and noise, are all included for particle matching to generate the displacement statistics, but are discounted during postprocessing by exploiting the fact that true particle-particle motion will observe a diffusive (Gaussian, or near-Gaussian) displacement distribution, while spurious particle-particle or particle-noise tracking will observe a uniform displacement distribution. As long as the number of particles tracked is large, and as long as the medium is uniform and isotropic, the width of the measured particle distribution function can be directly and accurately related to the MSD of a particle in the fluid [24].

In this paper, we use SPTV, as suggested by Guasto et al. [24], to overcome the difficulties in implementing traditional particle displacement measuring techniques. We present a microrheological assessment of the viscoelastic behavior of dilute concentrations of Methocel 90 HG - a long chain polymer that exhibits viscoelastic properties and low shear viscosities (up to 18 cP).

2. Experimental setup and procedure

The schematic of the experimental configuration is shown in Fig. 1A. The experimental system consists of an inverted epifluorescent microscope (Nikon ECLIPSE TE 2000 - U) equipped with a 100X oil immersion objective (Nikon, Plan Apo TIRF). A mercury lamp illuminates the sample and a epiflourescent filter set (Nikon 96320M) consisting of a low-pass excitation filter, a dichroic mirror and a high-pass emission filter is used to isolate the fluorescent microbeads suspended in the fluid sample. A high-speed CMOS camera (Photron Fastcam SA5) fitted with a image intensifier (Hamamatsu V9501U - 74 - G240) is used to record the particle motion at frame rates up to 1000 Hz.

A simple test fixture is fabricated using a small piece of Paraffin film (Parafilm M), cut into a square (~ 10 mm) with a small hole (~ 3 mm) punched through in the middle to create a test well. (The geometry of the test fixture is shown in Fig. 1B.) The film was placed upon a No. 1 coverglass (Fisher Scientific) and heated gently for 30 s until the film started to soften. A small volume (2 μL) of the test fluid was placed in the test well and sealed with a No. 1.5 coverslip (Fisher Scientific) on top. The sample is allowed to cool to room temperature for 5 min before the experiment commenced.

A 0.500% (wt/vol) Hydroxypropyl Methyl-cellulose (Methocel 90 HG, Sigma Aldridge) stock solution was prepared by dissolving the polymer in deionized water and rotating overnight at 200 rpm. Lower concentration solutions were diluted from the stock solution. The particle suspensions were prepared by diluting 200 nm and 100 nm fluorescent beads (Molecular Probes, Excitation/Emission: 540/560 nm) 500,000 times into each polymer solution.

To resolve the frequency-dependent viscoelastic moduli of the polymer solutions at various concentrations. Images were recorded at different framerates [17] ranging from 5 Hz to 1000 Hz using Photron FASTCAM Viewer (PFV) software. 2000 images were saved for each sample suspension and each experiment was repeated 3 times to reduce measurement errors and to ensure consistency.

3. Image analysis and data processing

Images were processed using custom software written in C++ and using the OpenCV library. A bilateral filter [28] was applied to the image to reduce background noise. This filter was used since it reduces the noise without sacrificing the sharp intensity gradient near edges of the imaged particles [29]. Following the application of the filter, the position of the centroid of each particle (including phantom particles due to background noise) was detected using the *contour* and *moment* functions in the OpenCV library.

To compute particle displacement distributions for a given time separation, Δt , the distance between all particles in the first image and all particles in the second image was computed. Unlike traditional particle tracking algorithms, there was no attempt to find likely particle pairs between the two images. This procedure was repeated for all image pairs separated by Δt , generating a distribution of particle displacements for each value of Δt . The distribution thus included all physical particle displacements, as well as "displacements" associated with random particle pairings as well as particle—noise and noise—noise pairings (see [24] for more details).

As suggested by Guasto et al. [24], the distribution of particle displacements in any direction R(t) should have the form of a modified Gaussian distribution with zero mean:

$$S(R,t) = C(t) + \frac{1}{\sqrt{2\pi\sigma(t)}} \exp(-\frac{(R-\mu(t))^2}{2\sigma(t)^2}),$$
 (1)

which is simply a Gaussian distribution plus a constant offset, or "table". The Gaussian part is due to the correlated particle displacements [30] while the table derives from phantom displacements recorded between un-correlated particle pairs and particle—noise pairs [24]. Since these parings are random the table has a uniform distribution. Note the mean-squared displacement (MSD) of particle dispersion is defined as

$$MSD(t) = \langle (R(t) - R(0))^2 \rangle = \langle R(t)^2 \rangle, \tag{2}$$

and by definition, the standard deviation $\sigma(t)$ of the Gaussian part in Eq. (1) is given as

$$\sigma(t) = \sqrt{\langle (R(t) - \mu(t))^2 \rangle}.$$
 (3)

Here, $\mu(t)$ represents the mean speed, or drift velocity of the flow field, which in the present case is close to 0. $\sigma(t)^2$ is then a good estimation of MSD(t).

The measured displacements histogram is fitted to Eq. (1) (using MATLAB's fitnlm function) to retrieve the MSD. The size of the interrogation window (l) is chosen to be larger than at least three times $\sigma_i(t)$ for each fitting process, otherwise the MSD is often overestimated.

3.1. Viscoelastic spectrum calculation

To accurately compute the relaxation time (τ) , we follow the method proposed by Mason et al. [12] which is repeated here for convenience. Assuming the fluid is isotropic and incompressible, the fluids viscoelastic spectrum $\widetilde{G}(s)$ is calculated as

$$\widetilde{G}(s) \approx \frac{k_B T}{\pi r M S D(t) \Gamma[1 + (\partial ln(MSD(t))/\partial ln(t))]} \Big|_{t=1/s}, \tag{4}$$

where k_B is the Boltzmann constant, T is the absolute temperature, r is the radius of the particle and Γ stands for the Gamma-function. We calculate the fluid's viscoelastic spectrum $\widetilde{G}(s)$ using the measured

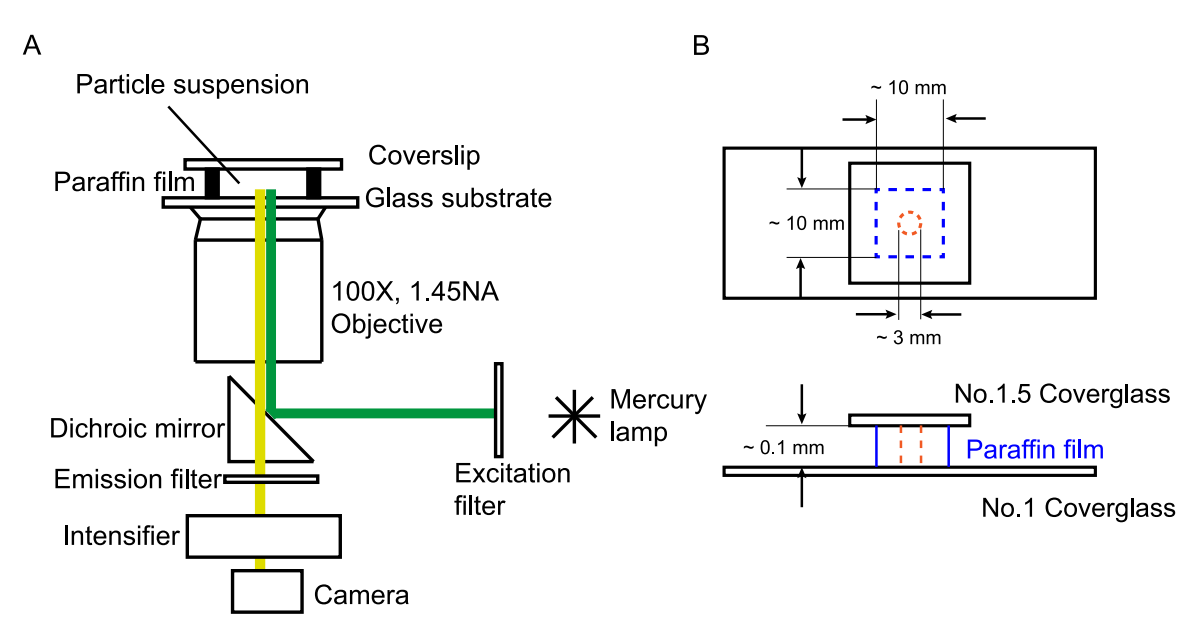


Fig. 1. A. Schematic of the experimental configuration. The tracer particles are illuminated using a mercury lamp with an excitation filter, the beam is introduced along the optical axis. The emission light follows the same light path until it reaches the dichroic mirror and passes through the emission filter. The light is captured via an image intensifier by a CMOS camera at up to 1000 fps; B. The geometry of the test fixture.

MSD vs. time. The partial derivative is numerically approximated using a first-order finite difference.

A non-linear curve fit of the resulting $\widetilde{G}(s)$ is performed to find the relaxation time(s), τ_i , and constant(s), G_i :

$$\widetilde{G}(s) = \sum_{i} \frac{G_{i}s}{s + 1/\tau_{i}}.$$
(5)

The storage (G') and loss (G'') moduli for polymer solutions at different concentration for each relaxation time are calculated as:

$$G'(\Omega) = \sum_{i} \frac{G_i \tau_i^2 \Omega^2}{1 + \Omega^2 \tau_i^2},\tag{6}$$

and

$$G''(\Omega) = \sum_{i} \frac{G_i \tau_i \Omega}{1 + \Omega^2 \tau_i^2}.$$
 (7)

4. Results and discussion

Sample images are shown in Fig. 2 illustrating the seeding particles (diameter: $200\,$ nm) in 0.125% Methocel solution. Fig. 2A1 and A2 are two consecutive images taken at $250\,$ fps, while images B1 and B2 are zoomed-in sections of each image denoted by the red squares, illustrating the interrogation window.

The procedure was first validated using water, a Newtonian fluid which should exhibit an MSD growing linearly with time. The displacement distributions of 100 and 200 nm particles were measured with Δt varying from 0.002–0.02 s. The MSD was computed using the SPTV technique described above, and the results are shown in Fig. 3. The slope of the measured MSD is in good agreement with the theoretical approximation based on the Stokes–Einstein equation [31], denoted by the solid lines.

With this reassurance, the MSDs of 200 nm particles suspended in Methocel solutions of different concentrations were measured, and are shown in Fig. 4. It is observed the MSD decreases as the polymer concentration increases indicating an increased viscous behavior. For long times the slope of MSD (on a log–log scale) is 1 for all concentrations used in the experiment, suggesting a diffusive behavior. At shorter times, however, the slope becomes less than 1 indicating the existence of elastic behavior in the fluid [12]. Moreover, it is directly observed from Fig. 4 that the crossover time (relaxation time), which is indicated

Table 1 Relaxation times for different Methocel concentrations, assuming one and two relaxation times (i = 1, 2).

reiaxation til	1100 (1 1,2)			
i = 1				
Conc.	τ_1 [ms]	G_1		
0.063	0.76	11.34		
0.125	2.99	6.76		
0.250	4.68	7.23		
0.500	9.00	3.39		
i = 2				
Conc.	τ_1 [ms]	G_1	τ_2 [ms]	G_2
0.063	0.76	11.34	1.00×10 ⁻⁹	1.00×10 ⁻³
0.125	3.13	6.65	4.53×10^{-6}	3.13×10^{-3}
0.250	4.70	7.20	2.42×10^{-5}	1.92×10^{-2}
0.500	8.99	3.46	5.43×10^{-4}	6.52×10^{-6}
0.500				

by the transition point when the slope of the curve becomes less than 1, increases with respect to polymer concentration.

It has been observed previously that for particle dispersion in non-Newtonian fluids, the shape of the displacement distribution has a Gaussian center, but a non-Gaussian tail [32,33]. This is particularly true when the time separation is close to polymer relaxation time. However, the non-Gaussian tail contributes only 5% to the total distribution [32], which introduces a subtle change to the estimated MSD as compared with the one found by assuming a pure Gaussian distribution. This effect is observed in this study, resulting in the overestimation of the distribution tail (Fig. 5B). However, since the key information required for the MSD is contained in the width of the distribution, and not the tail, the discrepancy is negligible, and we are able to ignore it in our analysis.

The relaxation time, τ_i , and viscoelastic moduli, G' and G'', were calculated as described above. The results are shown in Fig. 6 and Table 1. The relaxation time of the polymer solutions we tested increases as the concentration rises, which is indicated by the cross-over frequency of G' and G'' in Fig. 6. The calculation was carried out assuming both one and two relaxation times, although adding a second pair of fitting parameters (τ_2, G_2) had a negligible effect on the estimation of the longest time, τ_1 , and the modulus, G_1 (Table 1). This is also shown in the inset figure in Fig. 6D.

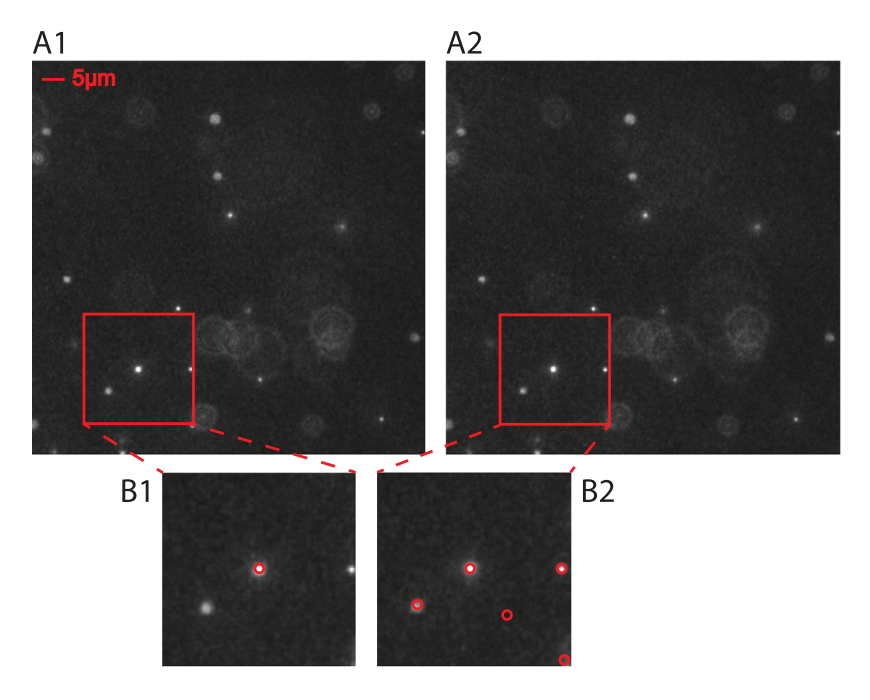


Fig. 2. Particles (200 nm) dispersion in 0.125% Methocel solution at two consecutive frames (A1 and A2). B1 and B2 are zoom-in images of the parts shown in A1 and A2 by a square (interrogation window) respectively. Circle marker in B1 shows the central particle and markers in B2 are all particles detected within the same interrogation window in the following image. The displacements are measured between all particles in B2 to the one in B1.

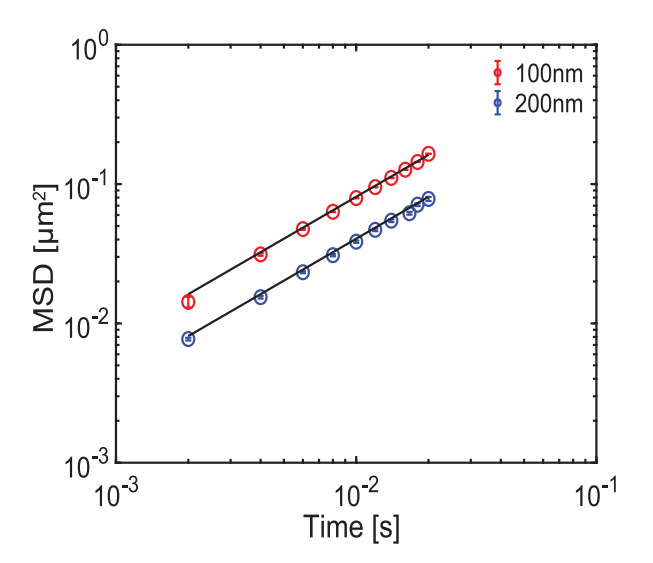


Fig. 3. MSD of diffusive particles in water. Particles with two sizes (100 nm and 200 nm) are tested to calibrate the measurement and processing algorithm. The black lines are estimated MSD over time theoretically using Stoke–Einstein equation. Temperature is $18\ ^{\circ}\text{C}$.

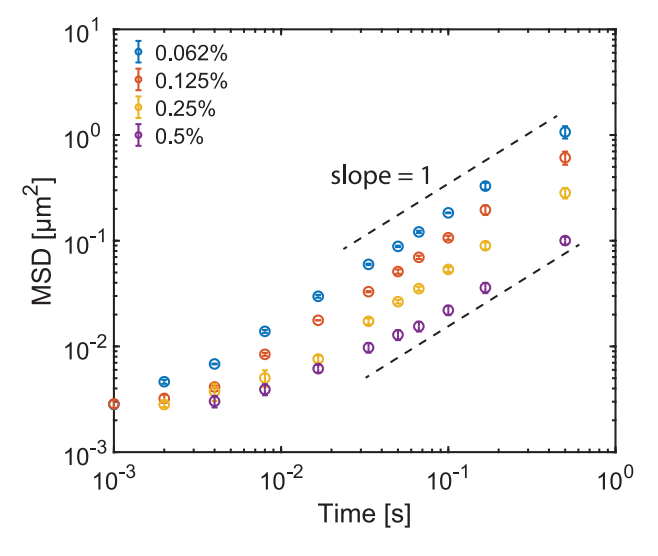


Fig. 4. MSD of particle dispersion in Methocel solutions at different concentrations as a function of time. The slope of MSD over time is 1 in four different concentrations at long time scale and becomes less than 1 at short time scale. In addition, the transition time increases with respect to polymer concentration.

5. Concluding remarks

Statistical Particle Tracking Velocimetry (SPTV) has been introduced and applied to a microrheology experiment as an alternative to more conventional particle tracking techniques. The advantages of SPTV are that it removes concerns regarding spurious particle tracking which is particularly problematic when tracking small particles with highly-amplified intensified images subject to noise. The data presented here demonstrate that the sampling frequency of microrheology measurement using intensified high speed image acquisition and fluorescent microscopy is effective at frequencies as high as 1 kHz, and thus extends beyond the spectrum that can be measured using a conventional

mechanical shear rheometer. The result indeed shows the relaxation time of dilute Methocel solutions, which is on the order to $10~\mathrm{ms}$, are short, and our result provides a robust basis for a complete study of the viscoelastic behavior of dilute polymer solutions.

Despite its appeal, this method has limitations. First, the rheology of the fluid is resolved at zero shear rate. Second, for solutions with higher viscosity, smaller-sized particles (or quantum dots) will be needed for displacement detection [24], which may not be guaranteed to observe the Stokes–Einstein relation even in Newtonian solutions [24]. Lastly, the SPTV method requires the MSD to observe a known distribution and this makes the technique difficult to implement in concentrated polymer solutions, where the distribution is non-Gaussian [32,33].

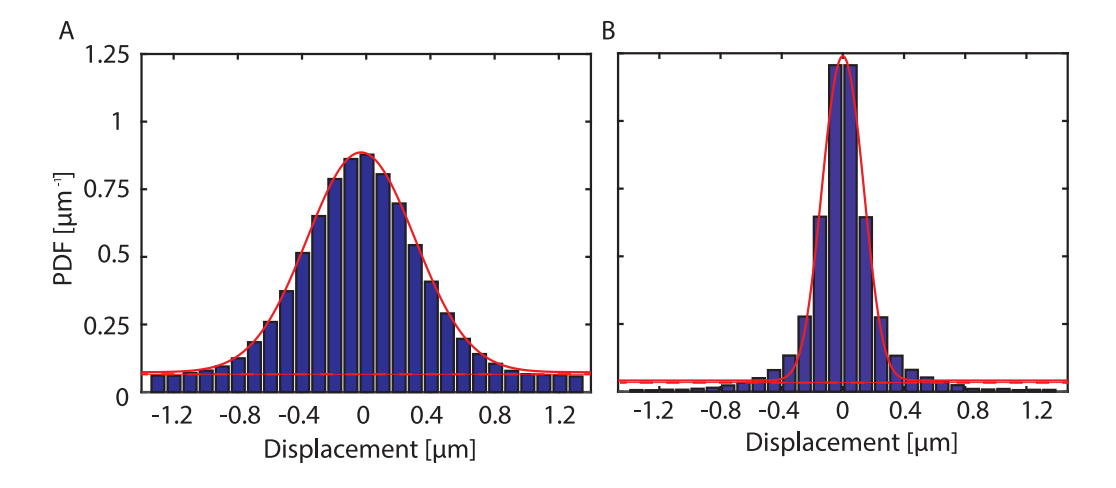


Fig. 5. Measured particle displacement distribution. A, the displacement distribution of 100 nm particle in water taken at 100 Hz. B, the displacement distribution of 200 nm particle in 0.125% Methocel solution take at 125 Hz. The solid red curves are the fitted Gaussian distribution and the dashed red lines indicate the constants used in each case.

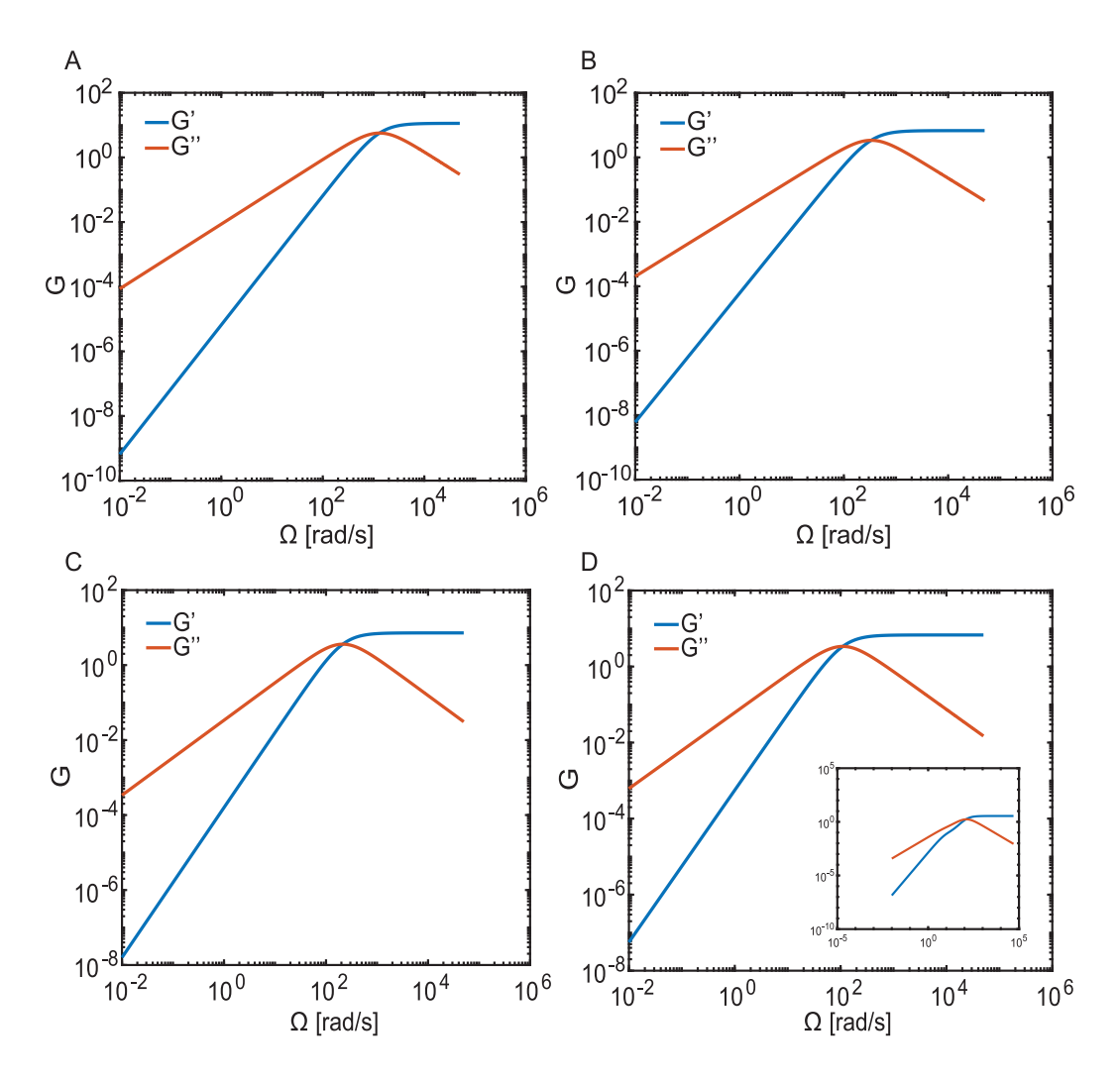


Fig. 6. Calculated elastic and viscous modulus of the Methocel solutions tested in the experiment at different concentration. A, 0.063% B, 0.125% C, 0.250% D, 0.500%. Inset D, 0.500% with two relaxation times. The non-linear fitting model assumes a single relaxation time as it is similar to the result of multiple relaxation time. The cross over point, which also indicates the relaxation time increases as a function of polymer concentration which is observed from Fig. 4.

However, the technique remains appropriate in dilute solutions exhibiting short relaxation times, which is precisely the regime where conventional rheometry has difficulties.

CRediT authorship contribution statement

Zijie Qu: Conceptualization, Methodology, Experiment, Writing – review & editing. **Xiongfeng Yi:** Methodology, Experiment. **Kenneth S. Breuer:** Conceptualization, Supervision, Writing – review & editing.

Declaration of competing interest

The authors declare that they have no known competing financial interests or personal relationships that could have appeared to influence the work reported in this paper.

Data availability

Data will be made available on request.

Acknowledgment

This work was supported by the National Science Foundation, USA, Grant (CBET 1336638)

References

- [1] C.D. Han, Rheology in Polymer Processing, Academic Press, 1976.
- [2] M. Baumgärtel, N. Willenbacher, The relaxation of concentrated polymer solutions, Rheol. Acta 35 (2) (1996) 168–185.
- [3] R.B. Bird, et al., Dynamics of Polymeric Liquids, Wiley, 1977.
- [4] R.D. Hester, D. Squire, Rheology of waterborne coatings, J. Coat. Technol. 69 (864) (1997) 109–114.
- [5] S.-i. Karato, Z. Wang, B. Liu, K. Fujino, Plastic deformation of garnets: systematics and implications for the rheology of the mantle transition zone, Earth Plan. Sci. Lett. 130 (1–4) (1995) 13–30.
- [6] A. Zettlemoyer, G. Lower, The rheology of printing inks. III. Studies of simple dispersions, J. Colloid Sci. 10 (1) (1955) 29–45.
- [7] F. Amblard, B. Yurke, A. Pargellis, S. Leibler, A magnetic manipulator for studying local rheology and micromechanical properties of biological systems, Rev. Sci. Instrum. 67 (3) (1996) 818–827.
- [8] G.R. Cokelet, E. Merrill, E. Gilliland, H. Shin, A. Britten, R. Wells Jr., The rheology of human blood—measurement near and at zero shear rate, Trans. Soc. Rheol. 7 (1) (1963) 303–317.
- [9] J.D. Ferry, Viscoelastic Properties of Polymers, John Wiley & Sons, 1980.
- [10] J.J. Crassous, R. Régisser, M. Ballauff, N. Willenbacher, Characterization of the viscoelastic behavior of complex fluids using the piezoelastic axial vibrator, J. Rheol. 49 (4) (2005) 851–863.

- [11] T.M. Squires, T.G. Mason, Fluid mechanics of microrheology, Annu. Rev. Fluid Mech. 42 (2010).
- [12] T. Mason, K. Ganesan, J. Van Zanten, D. Wirtz, S. Kuo, Particle tracking microrheology of complex fluids, Phys. Rev. Lett. 79 (17) (1997) 3282.
- [13] G. Fritz, W. Pechhold, N. Willenbacher, N.J. Wagner, Characterizing complex fluids with high frequency rheology using torsional resonators at multiple frequencies. J. Rheol. 47 (2) (2003) 303–319.
- [14] K.B. Arbogast, K.L. Thibault, B.S. Pinheiro, K.I. Winey, S.S. Margulies, A high-frequency shear device for testing soft biological tissues, J. Biomech. 30 (7) (1997) 757–759.
- [15] N. Willenbacher, C. Oelschlaeger, Dynamics and structure of complex fluids from high frequency mechanical and optical rheometry, Curr. Opin. Colloid Interface Sci. 12 (1) (2007) 43–49.
- [16] F. Crick, A. Hughes, The physical properties of cytoplasm, Exp. Cell Res. 1 (1) (1950) 37–80.
- [17] T.G. Mason, D. Weitz, Optical measurements of frequency-dependent linear viscoelastic moduli of complex fluids, Phys. Rev. Lett. 74 (7) (1995) 1250.
- [18] T. Mason, D. Weitz, Linear viscoelasticity of colloidal hard sphere suspensions near the glass transition, Phys. Rev. Lett. 75 (14) (1995) 2770.
- [19] B. Schnurr, F. Gittes, F. MacKintosh, C. Schmidt, Determining microscopic viscoelasticity in flexible and semiflexible polymer networks from thermal fluctuations, Macromolecules 30 (25) (1997) 7781–7792.
- [20] C.A. Murray, D.G. Grier, Video microscopy of monodisperse colloidal systems, Ann. Rev. Phys. Chem. 47 (1) (1996) 421–462.
- [21] D.P. Cattin, Image Restoration: Introduction to Signal and Image Processing, Vol. 11, MIAC, University of Basel, 2013, p. 93, Retrieved.
- [22] L. MacDonald, Digital Heritage, Routledge, 2006.
- [23] B. Qian, J. Park, K.S. Breuer, Large apparent slip at a moving contact line, Phys. Fluids 27 (9) (2015) 091703.
- [24] J.S. Guasto, P. Huang, K.S. Breuer, Statistical particle tracking velocimetry using molecular and quantum dot tracer particles, Exp. Fluids 41 (6) (2006) 869–880.
- [25] T. Schmidt, G. Schütz, W. Baumgartner, H. Gruber, H. Schindler, Imaging of single molecule diffusion, Proc. Natl. Acad. Sci. 93 (7) (1996) 2926–2929.
- [26] V. Levi, Q. Ruan, E. Gratton, 3-D particle tracking in a two-photon microscope: application to the study of molecular dynamics in cells, Biophys. J. 88 (4) (2005) 2919–2928.
- [27] E. Afik, Robust and highly performant ring detection algorithm for 3d particle tracking using 2d microscope imaging, Sci. Rep. 5 (2015) 13584.
- [28] B. Zhang, J.P. Allebach, Adaptive bilateral filter for sharpness enhancement and noise removal, IEEE Trans. Image Process. 17 (5) (2008) 664–678.
- [29] W. Jiang, M.L. Baker, Q. Wu, C. Bajaj, W. Chiu, Applications of a bilateral denoising filter in biological electron microscopy, J. Struct. Biol. 144 (1–2) (2003) 114–122.
- [30] T.G. Mason, Estimating the viscoelastic moduli of complex fluids using the generalized Stokes–Einstein equation, Rheol. Acta 39 (4) (2000) 371–378.
- [31] A. Einstein, Investigations on the Theory of the Brownian Movement, Courier Corporation, 1956.
- [32] E.R. Weeks, J.C. Crocker, A.C. Levitt, A. Schofield, D.A. Weitz, Three-dimensional direct imaging of structural relaxation near the colloidal glass transition, Science 287 (5453) (2000) 627–631.
- [33] T. Toyota, D.A. Head, C.F. Schmidt, D. Mizuno, Non-Gaussian athermal fluctuations in active gels, Soft Matter 7 (7) (2011) 3234–3239.